

Pulsed pump: Thermal effects in solid state lasers under super-Gaussian pulses

H NADGARAN and M SABAIAAN

Physics Department, College of Science, Shiraz University, Shiraz 71454, Iran

E-mail: nadgaran@susc.ac.ir

MS received 22 June 2006; revised 20 September 2006; accepted 18 October 2006

Abstract. Solid state laser (SSL) powers can be realistically scaled when pumped by a real, efficient and multimode pulse. In this work, a fourth-order super-Gaussian pulse was assumed as a pump for SSL's and a complete analytical expression for the thermal phase shift is given. Moreover, the focal length of thermal lens in paraxial ray approximation regime was studied. The results when applied to a Ti:sapphire crystal show an appreciable correction for aberration compared to a top-hat pulse.

Keywords. Pulse pump; thermal effects; thermal lensing; phase shift; diode-pumped solid state laser; super-Gaussian pump profile.

PACS Nos 42.55.Xi; 42.25.Lc

1. Introduction

Pulse laser systems have been developed and promoted by new and improved laser crystals. Strong thermal effects caused by the deposited heat in laser crystals introduce complications, that is, the laser crystal is greatly influenced by the heat; it limits the maximum pump power and makes its resonator unstable [1]. Subsequent cooling of the crystal medium with the associated thermal gradient would lead to a thermally-induced change of refractive index. Ti-doped sapphire is a suitable laser crystal which can be effectively pumped by short pulses. The combination of sapphire's excellent thermal, physical and optical properties with a material of tunable range has made it a very popular laser over the entire band of 660–1100 nm [2]. Many noticeable efforts for managing and reducing thermal effects under various types of pumping geometries are found in [3–7]. This work assumes a pulse pump of super-Gaussian of order four and it is essentially regarded as an extension to Farrukh *et al* [8] and Lausten and Balling [9] works who assume a top-hat profile for the pump. An analytical expression of temperature distribution for a cylindrical-shaped crystal pumped by a pulse of energy near its damage threshold will be given in §2. The thermal-induced overall phase-shift and its analytical form under the

paraxial ray approximation regime will be presented in §3 and the paper will be concluded by calculating the focal length of thermal lens.

2. Temperature distribution

The time-dependent heat transport equation is written as [2]

$$K\nabla^2 T - \rho c \frac{\partial T}{\partial t} = Q(\mathbf{r}, t), \quad (1)$$

where Q , K , ρ and c are heat source density, thermal conductivity, mass density and crystal specific heat, respectively.

For short pulses, the pulse duration is usually assumed smaller than the transfer time of the heat. So when the pulse is off, we can investigate eq. (1) with $Q(r, t) = 0$, that is,

$$\frac{\partial T}{\partial t} = \kappa \nabla^2 T, \quad (2)$$

where $\kappa = K/\rho c$ is defined as thermal diffusivity [10]. In cylindrical coordinate system, eq. (2) takes the form

$$\frac{\partial T(r, z, t)}{\partial t} = \kappa \left(\frac{\partial^2}{\partial r^2} + \frac{1}{r} \frac{\partial}{\partial r} + \frac{\partial^2}{\partial z^2} \right) T(r, z, t), \quad (3)$$

where $T(r, z, t)$ stands for the temperature difference of any point in the rod and the coolant temperature. Assuming a solution of the form $T(r, z, t) = f_1(r)f_2(z)f_3(t)$, we end up with three separated equation with the following solutions:

$$f_2(z) = A \sin(\mu z) + B \cos(\mu z), \quad (4)$$

$$f_3(t) = C \exp(-\kappa(\mu^2 + \nu^2)t), \quad (5)$$

where ν and μ are constants of separation and the solution of r -dependent part is recognized as a simple zero-order Bessel and Neumann functions [9].

3. Boundary and initial conditions – General solution

As the Neumann function diverges at $r = 0$, only the Bessel function contributes. Assuming a fixed temperature on the rod cylindrical boundary and neglecting heat loss from the ends of the crystal and desiring the derivative of the solution to vanish at the end points, one will be led to retain the cosine series [9]. By adapting an initial condition of $T(r, z, t = 0)$ and $T(r = a, z, t) = 0$, the following general solution for cylindrical rod of radius a and length l is obtained:

$$T(r, z, t) = \sum_{n=1}^{\infty} \sum_{m=0}^{\infty} A_{nm} J_0(r\alpha_n/a) \cos\left(\frac{m\pi}{l}z\right) \times \exp\left(-\kappa\left(\frac{\alpha_n^2}{a^2} + \frac{m^2\pi^2}{l^2}\right)t\right), \quad (6)$$

where α_n 's are the zeros of the Bessel function $J_0(r)$ and m is an integer. In the case of end pumping, the initial temperature profile is the same as the radiation profile and is written as [8]

$$T(r, z, t = 0) = \frac{E_0}{\rho c} \left[1 - \eta \frac{\lambda_{\text{pump}}}{\lambda_{\text{laser}}}\right] g(r, z) a(r, z), \quad (7)$$

where E_0 is the total energy of the pump pulse, λ_{pump} and λ_{laser} are the pump and laser wavelengths and η is the quantum efficiency. $g(r, z)$ is the normalized fourth-order super-Gaussian function observing the following relation:

$$\int_0^{\infty} \int_0^{\infty} 2\pi r g(r, z) dr dz = 1 \quad (8)$$

and $a(r, z)$ describes the absorption of heat in the rod. This $g(r, z)$ is calculated as

$$g(r, z) = \frac{2\sqrt{2}}{l\omega_p^2\pi^{3/2}} \exp(-2r^4/\omega_p^4), \quad (9)$$

where ω_p is the beam waist of the pump. As the amount of heat is reduced along the rod exponentially, one can simply assume that $a(r, z) = \exp(-\gamma z)$, where γ is the absorption coefficient of the crystal rod at the pump wavelength. The full expression for T at $t = 0$ is then

$$T(r, z, t = 0) = T_0 \exp(-2r^4/\omega_p^4) \exp(-\gamma z), \quad (10)$$

where T_0 , the temperature difference between the center of the rod and the coolant at $t = 0$, is

$$T_0 = \frac{2\sqrt{2}}{\pi^{3/2}} \frac{E_{\text{total}}}{\omega_p^2 \text{erf}(\sqrt{2}a^2/\omega_p^2) \rho c l} \left[1 - \eta \frac{\lambda_{\text{pump}}}{\lambda_{\text{laser}}}\right]. \quad (11)$$

The value of the erf function in the denominator of eq. (11) when inserting the values of a and ω_p into its argument becomes 0.998 which has been taken as unity.

One can multiply both sides of eq. (6) by $J_0(r\alpha_n/a)$ and $\cos(m'\pi z/l)$ and using the orthogonality properties of Bessel and cosine functions in integration over $r = 0 \rightarrow r = a$ and $z = 0 \rightarrow z = l$, to obtain:

$$A_{nm} = 4 \frac{\int_0^a dr \int_0^l dz T(r, z, t = 0) r J_0(r\alpha_n/a) \cos(\frac{m\pi}{l}z)}{a^2 l J_1^2(\alpha_n)}. \quad (12)$$

For $m = 0$ we use $\frac{1}{2}A_{nm}$.

The exponential factor under the summation sign of eq. (6) consists of a and l which are the maximum values of r and z respectively. So it is worth separating the r and z parts of $T(r, z, t)$ in eq. (6) further to obtain the time-dependent radial temperature as

$$T_r(r, t) = \sum_{n=1}^{\infty} B_n J_0(r\alpha_n/a) \exp(-\kappa\alpha_n^2 t/a^2), \quad (13)$$

where the expansion coefficient B_n can be obtained as

$$\begin{aligned} B_n &= \frac{2T_0 \int_0^a \exp(-2r^4/\omega_p^4) J_0(r\alpha_n/a) r dr}{a^2 J_1^2(\alpha_n)} \\ &= \frac{T_0 \exp(-2a^4/\omega_p^4)}{J_1^2(\alpha_n)} \sum_{s=0}^{\infty} \frac{(-\alpha_n^2/4)^s}{(s+1)(s+3)(s!)^2} \\ &\quad \times \left\{ \frac{4a^4}{\omega_p^4} {}_1F_1\left(1, \frac{5}{2} + \frac{s}{2}; \frac{2a^4}{\omega_p^4}\right) + s + 3 \right\}, \end{aligned} \quad (14)$$

where ${}_1F_1(a, c; x)$ is the confluent hypergeometric function defined as [11]

$${}_1F_1(a, c; x) = 1 + \frac{a}{c} \frac{x}{1!} + \frac{a(a+1)}{c(c+1)} \frac{x^2}{2!} + \dots, \quad c \neq 0, -1, -2, \dots \quad (15)$$

For a top-hat pump profile, which is used by Lausten and Balling [9], the following relation is fulfilled:

$$E_{th} = \frac{4E_0}{\pi a^2}, \quad (16)$$

where E_{th} is the maximum energy density needed to physically damage the crystal. In plotting figure 1, we finally need ω_p for our super-Gaussian pump profile. In order to calculate ω_p , one initially put $E_{th} = 1 \text{ J/cm}^2$ for Ti:sapphire [12] and $E_0 = 0.1 \text{ J}$ to calculate the proper crystal radius, a . As $r_p = a/2$, one can calculate the value of r_p for Lausten's case. Because we are willing to compare our results with Lausten's one, we take the area under his top-hat profile with r_p to be equal to the area under our super-Gaussian profile with ω_p . In this way, ω_p which is equivalent to r_p of Lausten will be calculated. The radial temperature of the crystal vs. r is plotted in figure 1 in the course of time after the first pulse. The time-dependent z -part of the temperature distribution is written as

$$T_z(z, t) = \frac{C_0}{2} + \sum_{m=1}^{\infty} C_m \cos\left(\frac{m\pi z}{l}\right) \exp\left(\frac{-\kappa m^2 \pi^2 t}{l^2}\right), \quad (17)$$

where C_m 's are

$$C_m = \frac{2}{l} \int_0^l \exp(-\gamma z) \cos\left(\frac{m\pi z}{l}\right) dz = \frac{2}{\gamma l} \frac{1 - \exp(-\gamma l) \cos(m\pi)}{1 + \left(\frac{m\pi}{\gamma l}\right)^2}. \quad (18)$$

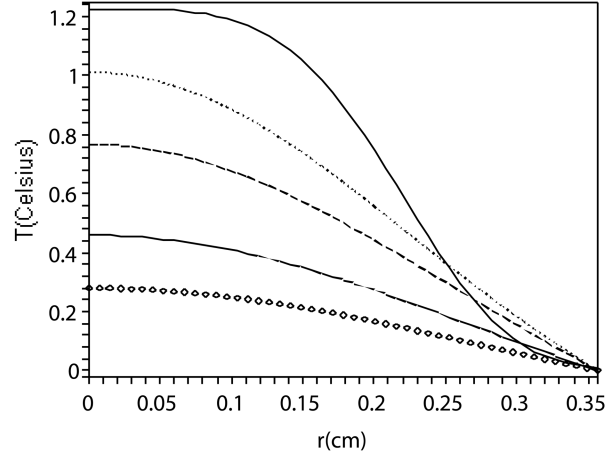


Figure 1. The radial temperature for initial profile of super-Gaussian at various times of $t = 0$ s, $t = 0.05$ s, $t = 0.1$ s, $t = 0.5$ s and $t = 1.0$ s seen from the top curve respectively. The parameters used are $l = 1$ cm, $E_0 = 0.1$ J, $a = 0.356$ cm, $\omega_p = 0.28$ cm, $\lambda_{\text{pump}} = 532$ nm, $\lambda_{\text{laser}} = 800$ nm and $\eta = 0.64$ [13].

As mentioned earlier, the pulse duration is assumed to be much smaller than that of the time needed for heat transfer over the rod, that is we used a single-shot. The rod will be hit by successive pulses, however, and one can add up the effects of the present and the previous shots as [9]:

$$T_{2^{\text{nd}} \text{ pulse}}(r, z, t) = T_r(r, t + \tau)T_z(z, t + \tau) + T_r(r, t)T_z(z, t), \quad (19)$$

where τ is the time between successive pulses. This leads to an expression of

$$\begin{aligned} T_{2^{\text{nd}} \text{ pulse}}(r, z, t) = & \frac{T_0}{2} \sum_{n=1}^{\infty} B_n C_0 J_0 \left(\frac{r \alpha_n}{a} \right) \exp \left(\frac{-\kappa \alpha_n^2 t}{a^2} \right) \\ & \times \left\{ 1 + \exp \left[-\kappa \left(\frac{\alpha_n^2}{a^2} \right) \tau \right] \right\} \\ & + T_0 \sum_{n=1}^{\infty} \sum_{m=1}^{\infty} B_n C_m J_0 \left(\frac{r \alpha_n}{a} \right) \cos \left(\frac{m \pi z}{l} \right) \\ & \times \exp \left[-\kappa \left(\frac{\alpha_n^2}{a^2} + \frac{m^2 \pi^2}{l^2} \right) t \right] \\ & \times \left\{ 1 + \exp \left[-\kappa \left(\frac{\alpha_n^2}{a^2} + \frac{m^2 \pi^2}{l^2} \right) \tau \right] \right\}. \end{aligned} \quad (20)$$

To find a steady-state solution, that is, when the number of pulses goes to infinity, we continue the procedure and soon found that the solution takes a closed form, because the expressions such as $1 + \exp(-\kappa \alpha_n^2 \tau / a^2)$ and $1 + \exp[-\kappa(\frac{\alpha_n^2}{a^2} + \frac{m^2}{l^2})\tau]$ take a geometric series form. Therefore, the temperature distribution after numerous pulse shootings will be

$$\begin{aligned}
 T_{\infty}(r, z, t) = & \frac{T_0}{2} \sum_{n=1}^{\infty} B_n C_0 J_0(r\alpha_n/a) \frac{\exp(-\kappa\alpha_n^2 t/a^2)}{1 - \exp[-\kappa(\frac{\alpha_n^2}{a^2})\tau]} \\
 & + T_0 \sum_{n=1}^{\infty} \sum_{m=1}^{\infty} B_n C_m J_0(r\alpha_n/a) \cos(m\pi z/l) \\
 & \times \frac{\exp[-\kappa(\frac{\alpha_n^2}{a^2} + \frac{m^2\pi^2}{l^2})t]}{1 - \exp[-\kappa(\frac{\alpha_n^2}{a^2} + \frac{m^2\pi^2}{l^2})\tau]}. \quad (21)
 \end{aligned}$$

4. Thermal effects

Here, thermo-optic effects such as dn/dT and end effects resulting from the local inhomogeneous temperature difference inside the rod will be investigated.

4.1 The dn/dT effect

To investigate the thermally-induced change of refractive index, one can expand $n(r, z, T)$ as

$$n(r, z, T) = n(r = 0, z, T) + \frac{dn}{dT}[T(r, z) - T(r = 0, z)] + \dots \quad (22)$$

This equation can be written as

$$\Delta n(r, z)_T = [T(r, z) - T(r = 0, z)] \frac{dn}{dT}, \quad (23)$$

where $\Delta n(r, z)_T = n(r, z, T) - n(r = 0, z, T)$.

This temperature-dependent change of refractive index can cause thermally-induced phase-shifts as [8]

$$\Delta\phi(r)_T = k \int_0^l \Delta n(r, z)_T dz, \quad (24)$$

where k is the wave number of the pump radiation source. Using eqs (24) and (21) phase-shifts at $t = 0$ will be

$$\Delta\phi(r)_T = \frac{T_0 C_0 l k}{2} \frac{dn}{dT} \sum_{n=1}^{\infty} B_n \frac{J_0(r\alpha_n/a) - 1}{1 - \exp[-\kappa(\alpha_n^2/a^2)\tau]}. \quad (25)$$

For using paraxial ray approximation (PRA) regime, we expand Bessel function as $J_0(r\alpha_n/a) = 1 - (r\alpha_n/2a)^2 + \dots$ and therefore the phase-shift becomes

$$\Delta\phi(r)_T \simeq -\frac{T_0 C_0 l k}{8} \frac{dn}{dT} \times \left(\frac{r^2}{a^2}\right) \sum_{n=1}^{\infty} \frac{B_n \alpha_n^2}{1 - \exp[-\kappa(\alpha_n^2/a^2)\tau]}. \quad (26)$$

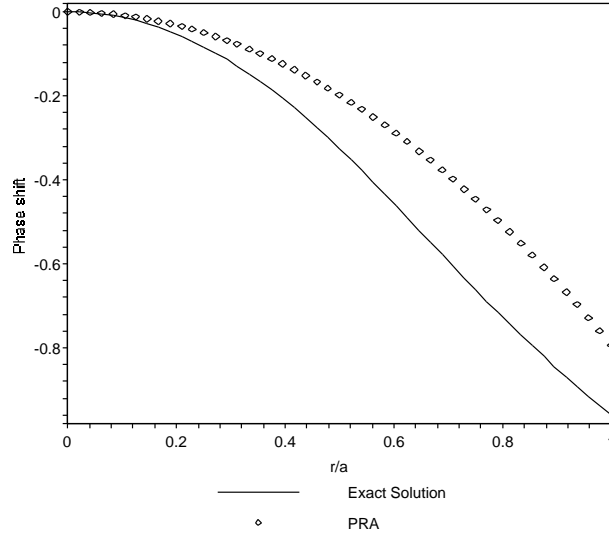


Figure 2. Exact phase-shift (solid) and paraxial ray approximation (dotted) are shown. The other parameters are the same as in figure 1.

Equations (25) and (26) show the exact phase-shift and its PRA approximation, respectively. Figure 2 shows these two equations as a function of r/a for $l = 1$ cm, $E_0 = 0.1j$, $\tau = 1 \times 10^{-2}$ s, $a = 0.35$ cm and $\omega_p = 0.28$ cm [9]. Figure 3 shows the expression $\Delta\phi(r)_{\text{Exact}} - \Delta\phi(r)_{\text{PRA}}$ vs. r/a with the same parameters. In this figure it is seen that, application of the above results on Ti:sapphire crystal (table 1) for region of $r/a \leq 0.5$ will give the deviation from the exact calculation of phase-shift even better than 0.02 of laser wavelength. So one can simply employ PRA framework and use a lens-like formula of

$$\Delta\phi(r)_T = -\frac{kr^2}{2f} \quad (27)$$

to calculate the focal length, f , of the thermal lens, i.e.

$$f_{\text{th}} \simeq \frac{4a^2}{T_0 C_0 l} \left\{ \frac{dn}{dT} \sum_{n=1}^{\infty} \frac{B_n \alpha_n^2}{1 - \exp(-\kappa \alpha_n^2 \tau / a^2)} \right\}^{-1}. \quad (28)$$

The variation of the focal length against the repetition frequency of the pulse, $\nu = 1/\tau$, is plotted in figure 4.

4.2 The end-effect

Axial expansion of the laser rod leads to curved end faces. This effect is referred to as end-effect. Elongation of the rod $L(r)$ is written as [14]

$$L(r) = \alpha_T \int_0^l [T(r, z) - T(r = 0, z)] dz, \quad (29)$$

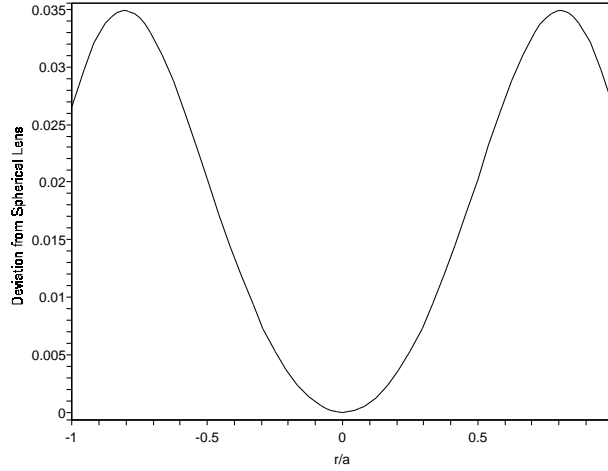


Figure 3. Deviation of PRA approximation calculation from the exact one in units of the laser wavelength (800 nm). The other parameters are the same as in figure 1.

Table 1. Thermal properties of Ti:sapphire at room temperature [15].

| Property | At 300°K |
|--------------------------------------|--|
| Thermal expansion coefficient | 5 (K ⁻¹ × 10 ⁻⁶) |
| Thermal conductivity | 0.33 (W cm ⁻¹ K ⁻¹) |
| Thermal dispersion dn/dT | 12.8 (K ⁻¹ × 10 ⁻⁶) |
| Absorption coefficient [9] | 2.5 (cm ⁻¹) |
| Volumetric heat capacity $C = c\rho$ | 3.1 (J cm ⁻³ K ⁻¹) |

where l and α_T are the length and thermal expansion coefficient of the crystal, respectively. Using eq. (21) elongation at $t = 0$ is obtained as

$$L(r) = \frac{T_0 C_0 l \alpha_T}{2} \sum_{n=1}^{\infty} B_n \frac{J_0(r \alpha_n / a) - 1}{1 - \exp[-\kappa(\alpha_n^2 / a^2) \tau]}. \quad (30)$$

Having $L(r)$, we can calculate the radius of curvature of the bent surface in the paraxial ray approximation using $R = -(d^2 L(r) / dr^2)^{-1}$ whose correspondent refractive focal length is given as [14]

$$f_{\text{ref}} = R / 2(n - 1), \quad (31)$$

$$f_{\text{ref}} \simeq \frac{1}{n - 1} \times \frac{2a^2}{T_0 C_0 l \alpha_T} \left[\sum_{n=1}^{\infty} \frac{B_n \alpha_n^2}{1 - \exp(-\kappa \alpha_n^2 \tau / a^2)} \right]^{-1}. \quad (32)$$

This expression is plotted vs. ν in figure 4. Figure 5 also shows the plot of the total focal length due to thermal and end-effect, i.e. $f = (1/f_{\text{th}} + 1/f_{\text{ref}})^{-1}$.

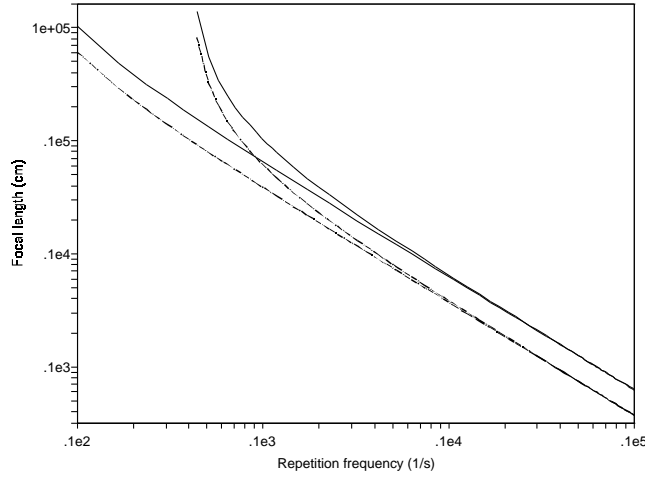


Figure 4. The end-effect focal length (solid) and the thermal focal length (dashed) are shown for two values of pulse peak energies of $E_0 = 0.1j$ (right curves) and $E_0 = 1j$ (left curves) vs. repetition frequency. The length of the crystal $l = 1$ cm. The other parameters, a and ω_p are chosen such that the energy of a top-hat pulse for $r_p = a/2$ is equal to the super-Gaussian one (see conclusion).

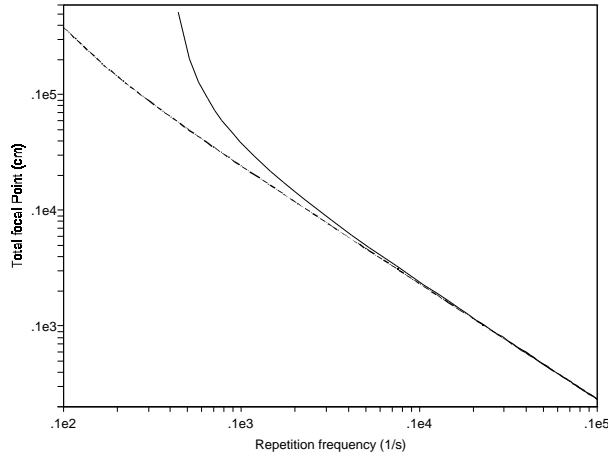


Figure 5. The total focal length $f = (1/f_{th} + 1/f_{ref})^{-1}$ is drawn for two values of pulse peak energies of $E_0 = 0.1j$ (solid) and $E_0 = 1j$ (dot) vs. repetition frequency $\nu = 1/\tau$. The other used parameters are the same as in figure 3.

5. Conclusion

A comparison between PRA and the exact calculation of the thermally-induced phase-shift inside the laser cavity (figure 3) proves that PRA approximation can

be easily and safely used to derive the focal length of the thermal lens; that is, one can assume a lens-like behavior inside the cavity when the crystal is pumped by a multi-mode super-Gaussian pulse. Figure 3 also shows that this deviation is nearly zero in the center of the rod, that is, if one concentrate the pump pulse on the center of the rod, even that tiny deviation would no longer be seen. One further result of figure 3 is that due to smooth variation of the super-Gaussian compared to top-hat, the deviation never becomes negative as in ref. [9]. Figure 4 shows the end-effect focal length and the thermal focal length vs. pulse repetition frequency for two distinct values of pulse energy. The results are comparable and agree with that of Lausten and Balling [9] in that, as the repetition frequency is increased, the focal length will be decreased considerably and the thermal effect would show itself in a more pronounced manner. This feature which was obtained for a pulse of super-Gaussian compared to Lausten top-hat pulse, would reveal the fact that a multi-mode pulse like a super-Gaussian used for high-power lasers cannot make the heat effects worse than the top-hat case. In comparing this work with Lausten, we assume that the total energy of a top-hat pulse close to the crystal damage threshold is equal to the total energy of a super-Gaussian pulse; that is, the area of a circle with radius $r_p = a/2$ was taken equal to $\int_0^a \exp(-2r^4/\omega_p^4) 2\pi r dr$. The above equality leads to $a/\omega_p \simeq 1.248$ in which a is the radius of the crystal rod and ω_p is the beam waist of the pump. Another important feature of figure 4 is that the two focal lengths have nearly the same order of magnitude; that is the end-effect should not be ignored. The total focal length is also depicted in figure 5 for the two peak energies of $0.1j$ and $1.0j$. The results are also in close agreement with Lausten and Balling [9]. We therefore believe a super-Gaussian profile is a more realistic profile which one can work with in the experimental.

References

- [1] A Nishimura, K Akaoka, A Ohzu and T Usani, *J. Nucl. Sci. Technol.* **38(12)**, 1043 (2001)
- [2] W Koechner, *Solid-state laser engineering*, 2nd ed. (Springer-Verlag, Berlin, 1988)
- [3] Yao Ai-Yun, Hou Wei and Li Hui-Qing, *Chin. Phys. Lett.* **22(3)**, 607 (2005)
- [4] R Weber, M P MacDonald, M B Ross and H P Weber, *IEEE J. Quantum Electron.* **34**, 1046 (1998)
- [5] T Graf, *SPIE Proc. Laser Resonators II LASE'99*, vol. 3611, p. 11 (1999)
- [6] T Graf *et al*, *Opt. Commun.* **135**, 171 (1997)
- [7] M MacDonald *et al*, *IEEE J. Quantum Electron.* **34**, 366 (1998)
- [8] U O Farrukh, A M Buoncristiani and C E Byvik, *IEEE J. Quantum Electron.* **24**, 2253 (1988)
- [9] R Lausten and P Balling, *J. Opt. Soc. Am.* **B20**, 1479 (2003)
- [10] H S Carslaw and J C Jaeger, *Conduction of heat in solids*, 2nd edn. (Oxford University, London, 1959)
- [11] G Arfken, *Mathematical methods for physicists*, 3rd edition (Academic Press, 1988)
- [12] F Canova, J P Chambaret, G Mourou, M Sentis, O Uteza, P Delaporte, T Itina, J Y Natoli, M Commandre and C Amra, *Proc. SPIE* vol. 5991, p. 639 (2005)
- [13] A Iseman, H Hundermark and C Fallnich, *Appl. Phys.* **B74**, 299 (2002)
- [14] M P MacDonald, Th Graf, J E Balmer and H P Weber, *Opt. Commun.* **178**, 383 (2000)
- [15] P A Schilz and S R Henion, *IEEE J. Quantum Electron.* **27**, 1039 (1991)